# Monte Carlo model to describe depth selective fluorescence spectra of epithelial tissue: applications for diagnosis of oral precancer

**Ina Pavlova**
Cornell University
School of Applied and Engineering Physics
Ithaca, New York 14853

**Crystal Redden Weber**
Rice University
Department of Chemistry
Houston, Texas 77005

**Richard A. Schwarz**
Rice University
Department of Bioengineering
Houston, Texas 77005

**Michelle Williams**
**Adel El-Naggar**
The University of Texas M. D. Anderson Cancer Center
Department of Pathology
Houston, Texas 77030

**Ann Gillenwater**
The University of Texas M. D. Anderson Cancer Center
Department of Head and Neck Surgery
Houston, Texas 77030

**Rebecca Richards-Kortum**
Rice University
Department of Bioengineering
Houston, Texas 77005

**Abstract.** We present a Monte Carlo model to predict fluorescence spectra of the oral mucosa obtained with a depth-selective fiber optic probe as a function of tissue optical properties. A model sensitivity analysis determines how variations in optical parameters associated with neoplastic development influence the intensity and shape of spectra, and elucidates the biological basis for differences in spectra from normal and premalignant oral sites. Predictions indicate that spectra of oral mucosa collected with a depth-selective probe are affected by variations in epithelial optical properties, and to a lesser extent, by changes in superficial stromal parameters, but not by changes in the optical properties of deeper stroma. The depth selective probe offers enhanced detection of epithelial fluorescence, with 90% of the detected signal originating from the epithelium and superficial stroma. Predicted depth-selective spectra are in good agreement with measured average spectra from normal and dysplastic oral sites. Changes in parameters associated with dysplastic progression lead to a decreased fluorescence intensity and a shift of the spectra to longer emission wavelengths. Decreased fluorescence is due to a drop in detected stromal photons, whereas the shift of spectral shape is attributed to an increased fraction of detected photons arising in the epithelium. 
[DOI: 10.1117/1.3006066]

Keywords: optical spectroscopy; tissue diagnostic; light propagation; Monte Carlo modeling.

Paper 07452RR received Nov. 6, 2007; revised manuscript received Aug. 27, 2008; accepted for publication Aug. 28, 2008; published online Nov. 5, 2008.

## 1 Introduction

Autofluorescence imaging of the oral cavity has emerged as a promising noninvasive technique to aid visualization and identification of premalignant and malignant oral lesions from benign lesions and normal oral mucosa.[1–4] Autofluorescence spectroscopy can also identify oral dysplasia and cancer with high specificity and sensitivity.[5–8] During neoplastic progression, the optical properties of both the superficial epithelium and the underlying stroma are altered. These changes can include an increase in epithelial cell scattering, increased stromal hemoglobin content, and decreased structural protein fluorescence within the stroma. Many research groups have developed analytical models to analyze fluorescence spectra collected *in vivo* in terms of these biochemical and morphologic changes.[6,9–12] Accurate biological interpretation of autofluorescence spectra of precancer and cancer diagnosis depends, in part, on prior knowledge of the key optical parameters associated with cancer progression, and a detailed understanding of how these optical parameters can alter the intensity and shape of the *in-vivo* spectra.

Interpretation of tissue spectra is made more complex because measured data often contain contributions from both the epithelium and stroma. Recently, a number of groups have developed fiber optic probes to acquire fluorescence spectra with depth selectivity.[13–15] Schwarz et al. used a ball-lens coupled probe to obtain spatially resolved fluorescence spectra from normal and neoplastic oral sites in a clinical setting.[16] The shallow channel of this probe has a source-detector separation of 720 $\mu$m. The ball-lens design allows fluorescence to be collected from approximately 300 $\mu$m beneath the probe surface, which corresponds primarily to the epithelium and the superficial stroma.

To guide the interpretation of spectra collected with such probes, we present a Monte-Carlo-based model to study the

Address all correspondence to: Rebecca Richards-Kortum, Department of Bioengineering, Rice University, 6100 Main St, Keck Hall Suite 116, Houston, Texas 77005. Tel: 713-348-5869; Fax: 713-348-5877; E-mail: rkortum@rice.edu

1083-3668/2008/13(6)/064012/13/$25.00 © 2008 SPIE

sensitivity of tissue fluorescence spectra collected with a depth-selective probe to variations in epithelial and stromal optical parameters associated with neoplastic transformation. An advantage of using Monte Carlo simulations rather than analytic models is the lack of simplifying assumptions, which must be made regarding either the source-detector geometry or the tissue heterogeneity. Monte Carlo simulations have been used to evaluate the effect of scattering and absorption changes on light propagation in a two-layer model of the cervix[17,18] and in multilayered models of the colon[19] and bronchial tissue.[20] As a clinically relevant example, we explore the application of this model to describe fluorescence spectra of oral tissue, using physiologically realistic input parameters and tissue geometries for normal oral tissue and for benign and precancerous oral lesions.

High-resolution fluorescence and confocal microscopy of viable oral tissue has elucidated the autofluorescence and scattering characteristics of the epithelial and stromal layers in normal, benign, and dysplastic tissue.[21–23] Results from these studies suggest that oral epithelium can be divided into three layers with different optical properties. The superficial oral epithelium is occupied by a highly scattering keratinized layer, which varies in thickness depending on the specific anatomical oral site or the presence of hyperkeratosis. The main fluorophore of the superficial layer is thought to be keratin. Beneath this layer, the nonkeratinized oral epithelium is less scattering and is occupied by metabolically active intermediate and basal cells. Fluorescence from the nonkeratinized epithelium is associated with the metabolic indicators NADH and FAD, which increase in dysplastic oral samples.[6,24]

Since carcinogenesis involves biochemical signaling between the epithelium and the surrounding extracellular matrix,[25] the optical properties of the superficial stroma are expected to be altered more by disease progression than those of the deeper stroma. Stromal fluorescence, caused by collagen and elastin cross-links, is significantly reduced in dysplastic and inflammatory oral samples, especially in the stromal layer immediately beneath the dysplastic epithelium. Dysplastic progression in oral mucosa leads to a decreased volume fraction of collagen and decreased stromal scattering,[26] which also may be more prominent in the superficial stroma. Angiogenesis, associated with neoplastic progression in oral mucosa,[27] may also be more prevalent in superficial stromal areas. In particular, spectra collected with a depth sensitive fiber optic probe will likely depend strongly on both the magnitude and the spatial extent of neoplastic-related changes in optical properties.

Here we introduce a Monte Carlo model to describe fluorescence spectra in oral mucosa with a multilayered tissue geometry, allowing depth-dependent variation in optical parameters in both the epithelium and stroma. This model uses realistic fluorescence input parameters for each sublayer derived from measurements in viable normal and neoplastic oral tissue. This depth sensitive model is used to study the sensitivity of predicted spectra to changes in biologically relevant optical parameters associated with the development of precancer and cancer, and thus to begin to elucidate the key optical parameters responsible for observed differences in normal and neoplastic fluorescence spectra. Finally, model predictions are compared to clinical spectroscopy measurements of normal and neoplastic tissue.

## 2 Methods

### 2.1 *Clinical Measurements of Fluorescence Spectra from Normal and Dysplastic Oral Mucosa*

A point probe spectroscopic system was used to obtain depth-resolved fluorescence spectra at 350-nm excitation of normal and neoplastic oral lesions in Institutional Review Board approved clinical studies carried out at the University of Texas M.D. Anderson Cancer Center.[16] Lesions selected by the clinician and an anatomically similar contralateral normal appearing site were measured for each patient by placing the probe against the mucosal surface. To minimize artifact from exposure to room light, the measurements were performed in a darkened room. Wavelength calibration, power calibration, and standard measurements were performed for each set of clinical measurements. After spectroscopic measurements, biopsies were collected from the corresponding tissue site for histological examination, subject to prior patient consent and discretion of the clinician. Histologic results were reviewed by a collaborating pathologist.

### 2.2 *Tissue Geometry and Model Input Parameters*

Oral mucosa is modeled as a multilayered medium with homogenous distribution of absorbers, scatterers, and fluorophores within each sublayer. As illustrated in Fig. 1(a), the epithelium of normal oral mucosa can be divided into three layers with different fluorescence characteristics.[21] The strongly scattering superficial epithelial layer includes cells that retain keratin, and the main fluorophore in this layer is assumed to be keratin. Immediately beneath this is a layer of intermediate nonkeratinized epithelial cells containing FAD as the dominant fluorophore. Beneath this is a layer of basal epithelial containing mitochondrial NADH as the dominant fluorophore. Similarly, the stroma can be divided into two layers with different optical properties: the superficial stroma and deeper stroma. Previous research shows that the main stromal fluorophores are collagen and elastin cross-links.[28] The thickness of each sublayer was derived from confocal fluorescence images of a representative normal tongue tissue slice that was used to determine the tissue geometry shown in Fig. 1(a). In our model, the total thickness of the epithelial layer is 280 $\mu$m; the superficial layer and the intermediate epithelial layer are each 80 $\mu$m thick, whereas the basal epithelial layer occupies 120 $\mu$m. The superficial stroma (stromal region 1) occupies an area 125 $\mu$m below the basement membrane, and deeper stroma (stromal region 2) is modeled as a semi-infinite medium.

In this model the fluorescence emission properties of a given sublayer are described by the fluorescence efficiency term $\mu(\lambda_{ex})\cdot\varphi(\lambda_{ex},\lambda_{em})$ of the dominant fluorophore within that sublayer, where $\mu(\lambda_{ex})$ is the absorption coefficient and $\varphi(\lambda_{ex},\lambda_{em})$ is the quantum efficiency of the dominant fluorophore. The relative magnitude of the fluorescence efficiency term for each sublayer was determined from the confocal images of the representative normal tongue tissue slice, used here as a baseline example. The spectral shape of the quantum efficiency for each sublayer was estimated from emission spectra at 350-nm excitation of biological samples containing the predominant fluorophore and not directly from the confocal images of the representative oral slice. The spectrum of keratin was obtained by measuring the fluorescence of human

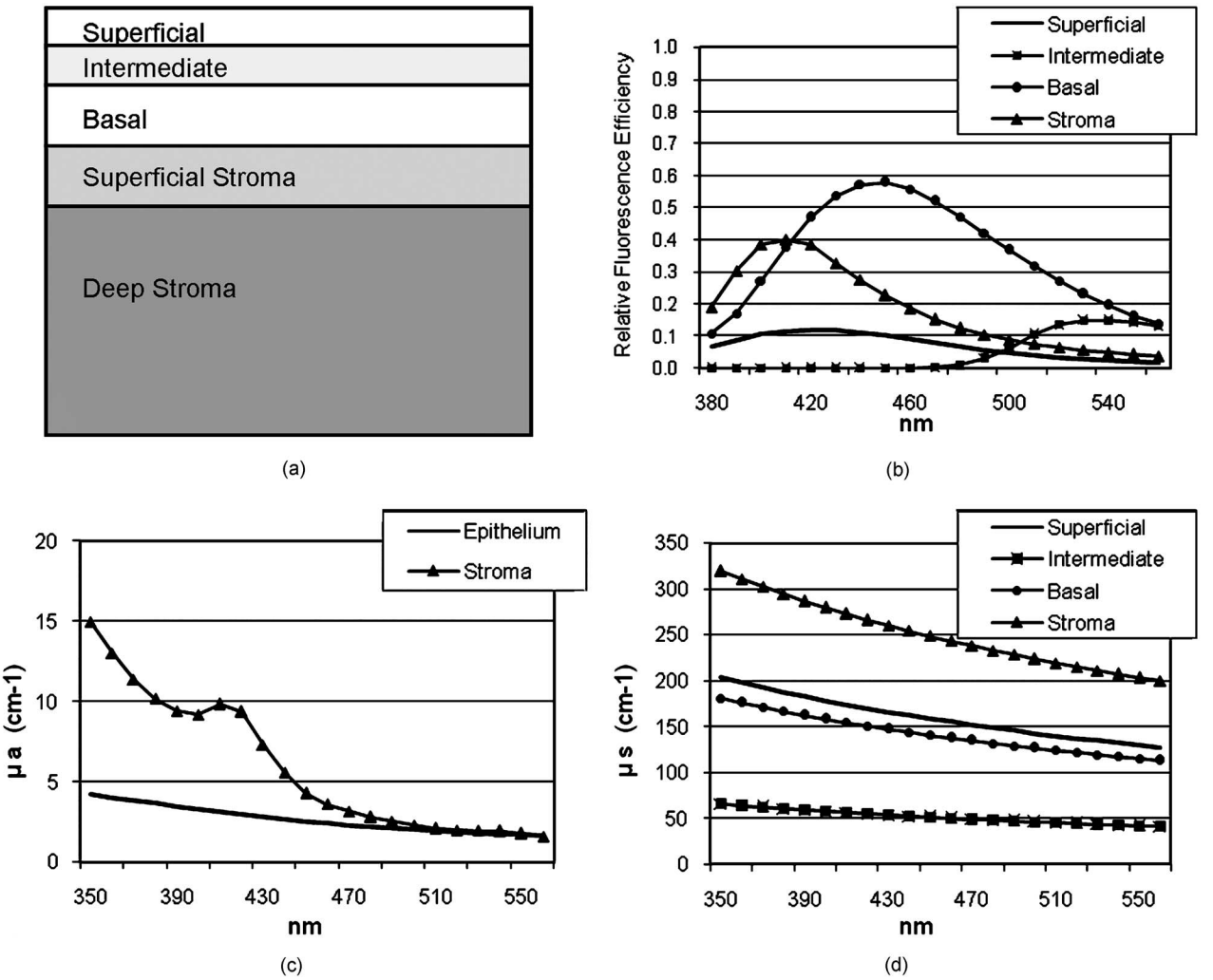


**Fig. 1** Baseline tissue geometry and input parameters. (a) Tissue geometry for normal oral tissue; superficial epithelial layer 80 $\mu$m, intermediate epithelial layer 80 $\mu$m, basal epithelial layer 120 $\mu$m, superficial stroma 125 $\mu$m, and deep stroma 1 cm. (b) Normalized fluorescence efficiencies. (c) Absorption coefficients. (d) Scattering coefficients.

which is dominated by keratin.[28] The emission spectrum of an optically dilute solution of FAD was used to represent the shape of the fluorescence efficiency of the intermediate epithelial cells. The fluorescence from a suspension of SiHa cervical cancer cells[28] was used to describe the shape of the basal epithelium. To ensure that fluorescence from the cell suspension is a valid approximation for fluorescence from basal epithelium, SiHa cells were grown on coverslips and imaged under the same conditions as oral tissue slices. SiHa cells displayed similar autofluorescence patterns as basal oral epithelium: cellular autofluorescence that is bright at UV excitation, but dimmer at 488-nm excitation. Next, a viable oral tissue slice was obtained that consisted of normal basal epithelium [the stroma and the rest of the epithelium were removed with a Krumdieck tissue slicer (Alabama Research and Development, Munford, Alabama)], and an emission spectrum of this sample was measured at 350-nm excitation. Comparisons of the emission spectra from basal epithelium and SiHa cell suspension showed that the two samples have very similar spectral shapes and emission peaks. Previously, it was shown that the emission spectrum from collagen type-1 gel can be described as a linear combination of spectra from three main types of collagen cross-links.[28] The contribution from collagen cross-links with emission peaks at 410 nm was found to be dominant, and was used here as input for the shape of the stromal fluorescence efficiency. The relative fluorescence efficiencies for each sublayer are summarized in Fig. 1(b).

Baseline values for the absorption and scattering coefficients for each epithelial and stromal layer were obtained from previous studies of cervical, oral, and bronchial tissue. The scattering coefficients of the superficial and basal epithelial layer were derived from reflectance confocal measurements of cervical epithelium.[22] In particular, the scattering coefficient extracted from keratinized cervical epithelium is used to represent superficial oral scattering, while the scattering coefficient from basal cervical cells is used here for the basal epithelial layer. The scattering coefficient of the intermediate epithelial layer was derived from reflectance confocal images of normal oral epithelium.[23] The stromal scattering coefficients for stromal layers 1 and 2 were assumed to be the same and were taken from a study on bronchial tissue.[29] Note

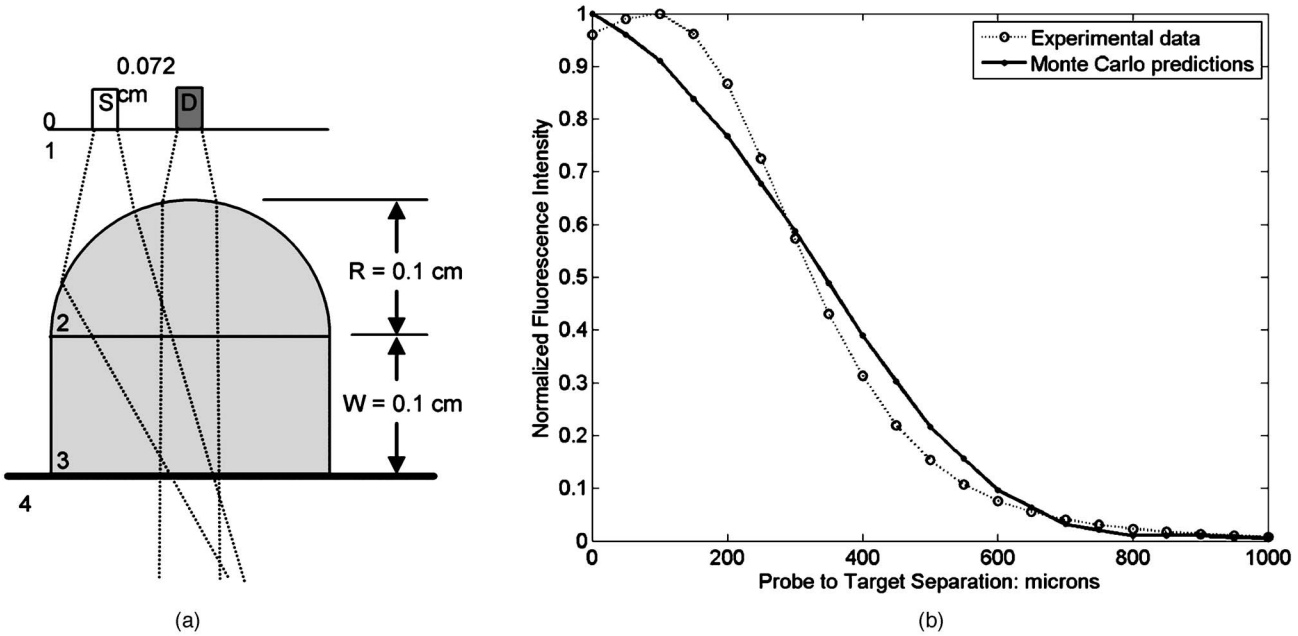


**Fig. 2** (a) Diagram of the depth selective fiber optic probe geometry used in the Monte Carlo forward model. S represents the source fiber and D the detector fiber. An air gap separates the fibers and the half ball lens. The distance between the source and detector fibers is 0.072 cm. The window is placed in contact with tissue. (b) Detected fluorescence intensity from a thin fluorescent layer, as the separation between the target and window is varied. The dotted line represents experimental data and the solid line represents the Monte Carlo predictions.

that the scattering coefficients were extrapolated to lower wavelengths using the inverse proportionality relationship of cellular scattering to wavelength.[30] The absorption coefficient was assumed to be constant throughout the oral epithelium and was based on measurements from bronchial tissue.[29] Stromal absorption is assumed to be caused by collagen and oxy- and deoxyhemoglobin. The total hemoglobin absorption coefficient was calculated by the well-known expression for blood absorption published by Jacques.[31] The extinction coefficients for oxy- and deoxyhemoglobin were taken from the same source, and the oxygen saturation of hemoglobin was assumed to be 80%. The concentration of hemoglobin per liter of blood used in this study was 150 g/l, the normal value reported by Jacques,[31] and the baseline volume fraction of blood in stromal layers 1 and 2 was set to be 0.16%. This fraction is very similar to values used in a previous model of light propagation in cervical and colon tissue.[17,32] In addition, Jacques reported a typical value for the blood volume fraction in skin (dermis) to be 0.2%.[31] To verify that a value of 0.16% is appropriate to describe blood absorption in oral mucosa, we have estimated the fraction of stroma occupied by the lumen of blood vessels from hematoxylin and eosin (H and E) slides of a representative normal and dysplastic oral tissue slice. Fractions derived from stromal areas 100 to 300 $\mu$m below the basement membrane are in agreement with the value used in this model. Stromal collagen absorption coefficients are based on measurements from bloodless skin samples.[33] Figures 1(c) and 1(d) summarize the baseline absorption and scattering coefficients for the stromal and epithelial layers used in this study.

### 2.3 *Description and Validation of the Monte Carlo Model of Fluorescence*

A fixed weight, multilayered reflectance Monte Carlo code with a depth selective fiber optic probe has been modified to account for generation and propagation of fluorescent light. Details regarding the reflectance Monte Carlo code and the geometry of illumination and collection are described in a previous study.[15] In the fluorescence Monte Carlo code used here, excitation photons are initially propagated using scattering and absorption coefficient values at the excitation wavelength. At each scattering event, the probability of the photon being absorbed is given by $\mu_a/(\mu_a+\mu_s)$, where $\mu_a$ is the absorption coefficient and $\mu_s$ is the scattering coefficient for a specific layer. On absorption, the probability that a photon is absorbed by a fluorophore is calculated. In the epithelial layers, this probability is equal to one, because it is assumed that the only absorbers are also fluorophores. In the stromal layers, however, a photon can be absorbed by either collagen cross-links (a fluorophore) or by hemoglobin (an absorber). The probability that the photon is absorbed by a stromal fluorophore is given by $\mu_a\text{coll}/(\mu_a\text{coll}+\mu_a\text{Hb})$, where $\mu_a$ coll is the absorption coefficient of collagen and $\mu_a$ Hb is the absorption coefficient for a given stromal layer at the excitation wavelength. The probability of fluorescence emission at a particular emission wavelength is given by the fluorescence efficiency of each sublayer. After isotropic emission, fluorescence photons are further propagated using the scattering and absorption coefficient of each layer at the emission wavelength, until reabsorbed or remitted from the tissue surface. The Heyney-Greenstein approximation was used as the phase

function.[34] The accuracy of the multilayered fluorescence Monte Carlo code for an infinite source and detector was compared to remitted fluorescence reported in the literature, and our results were found to be within 1% of published values.[35]

Figure 2 shows a diagram of the depth selective probe used to measure tissue fluorescence spectra and the geometry used within the Monte Carlo code. In the probe, a ball lens is used to confine illumination and collection to a shallow area, approximately 300 $\mu$m beneath the tissue surface. In the Monte Carlo code, the ball lens was approximated using a half ball lens coupled to a flat window.[15] To validate the depth selectivity of the Monte Carlo code, simulations of a thin fluorescent target were performed as a function of the distance between the detector and the target. Results were compared to experimental measurements. The experimental measurements were performed in water to better simulate the refractive index mismatch between the probe tip and tissue. In the simulations, the fluorescence target was modeled as a very thin (10 $\mu$m) strongly fluorescent layer, with a large absorption coefficient and a very small scattering coefficient, and a refractive index equal to 1.4. The gap between the probe and the target was represented by a layer with the optical properties of water. Simulations of measurements at different probe-to-target distances were performed by increasing the thickness of the water layer in increments of 50 to 100 $\mu$m.

### 2.4 *Predictions of Tissue Fluorescence Using the Monte Carlo Model*

After validation, the Monte Carlo model was then used to explore the predicted fluorescence spectra of tissue. All simulations were done at an excitation wavelength of 350 nm. A single simulation output consists of the detected fluorescence intensity (total number of detected fluorescence photons) at emission wavelengths of 400, 420, 440, 450, 460, 480, 500, 520, 540, and 560 nm. Each simulation was performed with $10^8$ excitation photons. Simulations were performed first for a baseline case using the optical properties of normal oral mucosa. Then a sensitivity analysis was performed by varying the optical properties of individual layers that are expected to change with neoplasia. In the baseline case and the model sensitivity analysis of stromal input parameters, simulations were repeated three times. Simulations for the model sensitivity analysis of epithelial parameters were performed only once.

For each detected photon, the depth at which fluorescence emission occurred was recorded. The mean depth of fluorescence was calculated by averaging these depths for all detected photons. To analyze the origin of the detected fluorescence signal at each emission wavelength, we calculated the fraction of detected photons with a depth of emission originating from the epithelium and the stroma, and also the fraction of detected photons originating from the superficial oral mucosa (the epithelium and stromal layer 1).

## 3 Results

### 3.1 *Validation of Model with Probe-to-Target Measurements in Water*

Figure 2 shows simulated fluorescence measurements for a thin fluorescent target as the distance between the probe tip and the sample is varied, and compares the performance of the modeled probe to the actual probe used in clinical studies. The relative error between predictions and experimental data is on average small, varying from 0.01 to 0.24 in the 0 to 400 $\mu$m range, and illustrates the depth selective nature of the probe, which collects fluorescence generated within 300 to 400 $\mu$m of the probe tip.

**Table 1** Effect of input parameters associated with hyperkeratosis, hyperplasia, and dysplasia on the fraction of photons detected from the epithelium and the fraction of photons detected from the superficial oral mucosa (the epithelium and superficial stroma) at emission wavelength of 440 nm.

| | Fraction of epithelial photons | Fraction of superficial photons |
|---|---|---|
| Baseline case | 0.43±0.01 | 0.90±0.01 |
| Thickness of nonkeratinized epithelium | | |
| −50 $\mu$m | 0.35 | 0.88 |
| +50 $\mu$m | 0.51 | 0.92 |
| +150 $\mu$m | 0.66 | 0.93 |
| Thickness of superficial epithelial layer | | |
| −50 $\mu$m | 0.38 | 0.89 |
| +50 $\mu$m | 0.50 | 0.90 |
| Thickness of the basal epithelial layer | | |
| −50 $\mu$m | 0.35 | 0.88 |
| +50 $\mu$m | 0.56 | 0.92 |
| +80 $\mu$m | 0.60 | 0.93 |
| Fluorescence Intensity of superficial stroma | | |
| Increased by 20% | 0.39 | 0.91 |
| Decreased by 20% | 0.50 | 0.89 |
| Decreased by 40% | 0.56 | 0.86 |

### 3.2 *Sensitivity of the Fluorescence Model to Variations in Epithelial Input Parameters*

The development of neoplasia in the oral cavity is accompanied by a series of physiological changes in the epithelium such as hyperkeratosis and higher cellular metabolic activity. These physiologic changes lead to changes in optical properties, including increased epithelial scattering and an increase in the NADH associated fluorescence from epithelial cells. The effect of each of these changes on the detected fluorescence was studied individually by varying a particular input parameter while holding all other factors constant. Figure 3 summarizes the predicted fluorescence spectra for three different sets of simulations designed to model hyperplasia, hyperkeratosis, and dysplasia in oral mucosa. Predictions in Figs. 3(a), 3(c), and 3(e) were normalized to the maximum

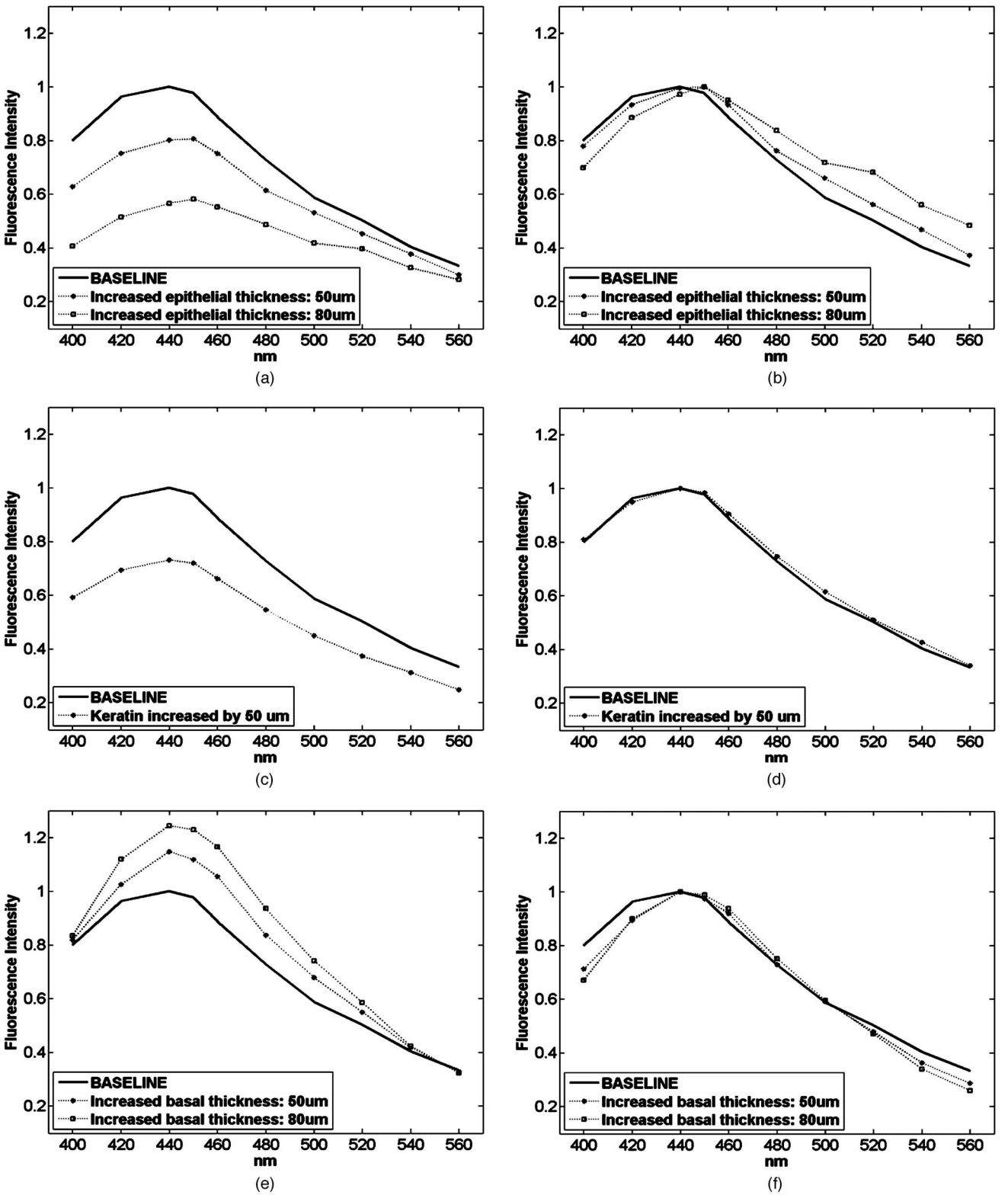


**Fig. 3** Effect of epithelial input parameters, associated with (a) and (b) hyperplasia, (c) and (d) hyperkeratosis, and (e) and (f) dysplasia on the intensity (left column) and spectral shape (right column) of the predicted fluorescence spectra.

intensity value of the baseline spectra (black line) to emphasize the effect of varying a particular input parameter on the overall intensity of the fluorescence. Predictions in Figs. 3(b), 3(d), and 3(f) were normalized by dividing each individual spectrum by its maximum intensity value to emphasize changes in spectral shape. In all sets of simulations, the baseline fluorescence spectrum is plotted as a black line. Table 1 summarizes the fraction of detected fluorescence photons that originate in the epithelium at 440-nm emission for each predicted spectrum.

The effect of hyperplasia is simulated by changing the thickness of the nonkeratinized epithelium (keeping the thickness of the superficial layer and the ratio of the intermediate epithelium to the basal epithelium thickness constant) in increments of 50 $\mu$m. Figures 3(a) and 3(b) show that, as the thickness of the nonkeratinized epithelium is increased, the overall fluorescence intensity drops, accompanied by a shift of the spectra to longer emission wavelengths and an increase in the fraction of detected photons generated in the epithelium. For example, increasing epithelial thickness by 150 $\mu$m results in a drop of fluorescence intensity at 440-nm emission by about a factor of 1.5, and an increase in the fraction of epithelial photons by about a factor of 1.6. Examination of the number of epithelial and stromal photons indicates that the relative increase in the fraction of epithelial photons is due more to a drop in stromal photons than to an increased number of epithelial photons. Increasing the thickness of the nonkeratinized epithelium decreases excitation light penetration to stromal areas, and thus increases sampling of epithelial fluorescence. Decreased epithelial thickness results in the opposite trend. It is interesting to observe that even small changes (50 $\mu$m) in the thickness of nonkeratinized epithelium have a significant effect on both the intensity and shape of the predicted spectra.

The effect of hyperkeratosis on the spectral shape and fluorescence intensity was studied by changing the thickness of the strongly scattering, keratinized superficial layer (and hence changing the total thickness of the epithelium) by 50 $\mu$m. Results are illustrated in Figs. 3(c) and 3(d). A thicker keratin layer results in a drop of fluorescence intensity by a factor of 1.3 without a significant shift in spectral shape and fraction of epithelial photons. However, a thicker keratin layer causes a small increase in photons detected from the keratin layer, and a large decrease in the numbers of photons from the underlying basal epithelial layer and stroma. Decreasing the thickness of the superficial layer has the opposite effect, due to deeper light penetration and increased detection of stromal fluorescence.

The development of dysplasia is associated with an increase in epithelial scattering and an increase in NADH-based cellular fluorescence. We have modeled these changes by increasing the thickness of the basal epithelial layer without changing the overall thickness of the epithelium. As shown in Figs. 3(e) and 3(f), an 80-$\mu$m increase in the thickness of the basal epithelium leads to higher total fluorescence intensity and a shift of the spectral shape to the red. These changes are accompanied by a significant increase (a factor of 1.4) in the fraction of detected epithelial photons, due an increase in the number of epithelial photons, but no significant change in the number of detected stromal photons. Thus, as the fraction of cells with higher scattering and NADH-based fluorescence increases, fluorescence from the epithelium starts to dominate the total detected fluorescence.

### 3.3 *Sensitivity of the Fluorescence Model to Variations in Stromal Input Parameters*

The fraction of epithelial photons, calculated for different sets of simulations and summarized in Table 1, indicates that the modeled probe detects a substantial number of stromal photons. For example, in the baseline case, more than half of the detected photons originate from the stroma. In tissue geometries representing hyperplasia and dysplasia, the fraction of epithelial photons rises to 0.60 to 0.66; however, complete rejection of stromal photons is not achieved, suggesting that variations in stromal parameters can also influence simulations. Here we have modeled stroma as a two layered medium, which allows us to study variations in input parameters within each individual stromal sublayer.

Figure 4 illustrates the effect of changing the magnitude of the stromal fluorescence efficiency on the total intensity and spectral shape of the predictions. Benign and dysplastic alterations in oral tissue were found to be characterized by a large drop of fluorescence intensity in the superficial stroma.[21] We simulated the effect of changes in the magnitude of the fluorescence efficiency of superficial stromal layer 1 [Figs. 4(a) and 4(b)], separately from changes in the deeper stromal layer 2 [Figs. 4(c) and 4(d)]. Decreasing the fluorescence efficiency of stromal layer 1 leads to a drop in the total fluorescence intensity and a shift of the spectrum to the red. These changes are also associated with an increased epithelial fraction of photons, due to a decrease in the number of stromal photons. Note that decreasing the fluorescence of stromal layer 1 by 40% leads to a significant decrease in total fluorescence (by a factor of 1.4 at 440 nm) and a relatively large increase in the fraction of epithelial photons (by a factor of 1.3). Previous research indicates that with inflammation and dysplasia, fluorescence from the stroma can drop by more then a factor of 3.[21] Thus, changes in the magnitude of the fluorescence efficiency of stromal layer 1 can have a potentially more significant effect than shown in Fig. 4. Decreasing the fluorescence efficiency of stromal layer 2 by 40% has only a small effect (less than 10%) on the spectral shape, fluorescence intensity, or the fraction of detected epithelial photons. This indicates that only changes in the magnitude of the fluorescence efficiency of stromal layer 1 lead to changes in predicted spectra collected with the depth selective probe.

The effect of changes in stromal hemoglobin absorption on predictions is illustrated in Fig. 5. An increase in blood vessel density by about a factor of 1.2 to 3 is commonly associated with premalignant progression in oral mucosa.[36] Here the volume fraction of hemoglobin in stroma was varied, which changes the stromal absorption coefficient. Simulations show that an increased volume fraction of hemoglobin in stromal layer 1 leads to a decrease in the total fluorescence intensity, mainly in the 400- to 440-nm emission region. These changes are also associated with small differences in the epithelial fraction of photons, also limited to the 400- to 450-nm emission range (data not shown). Changes in stromal layer 2 have a minimal effect on predicted spectra. Figure 6 summarizes the effect of decreasing scattering in stromal layers 1 and

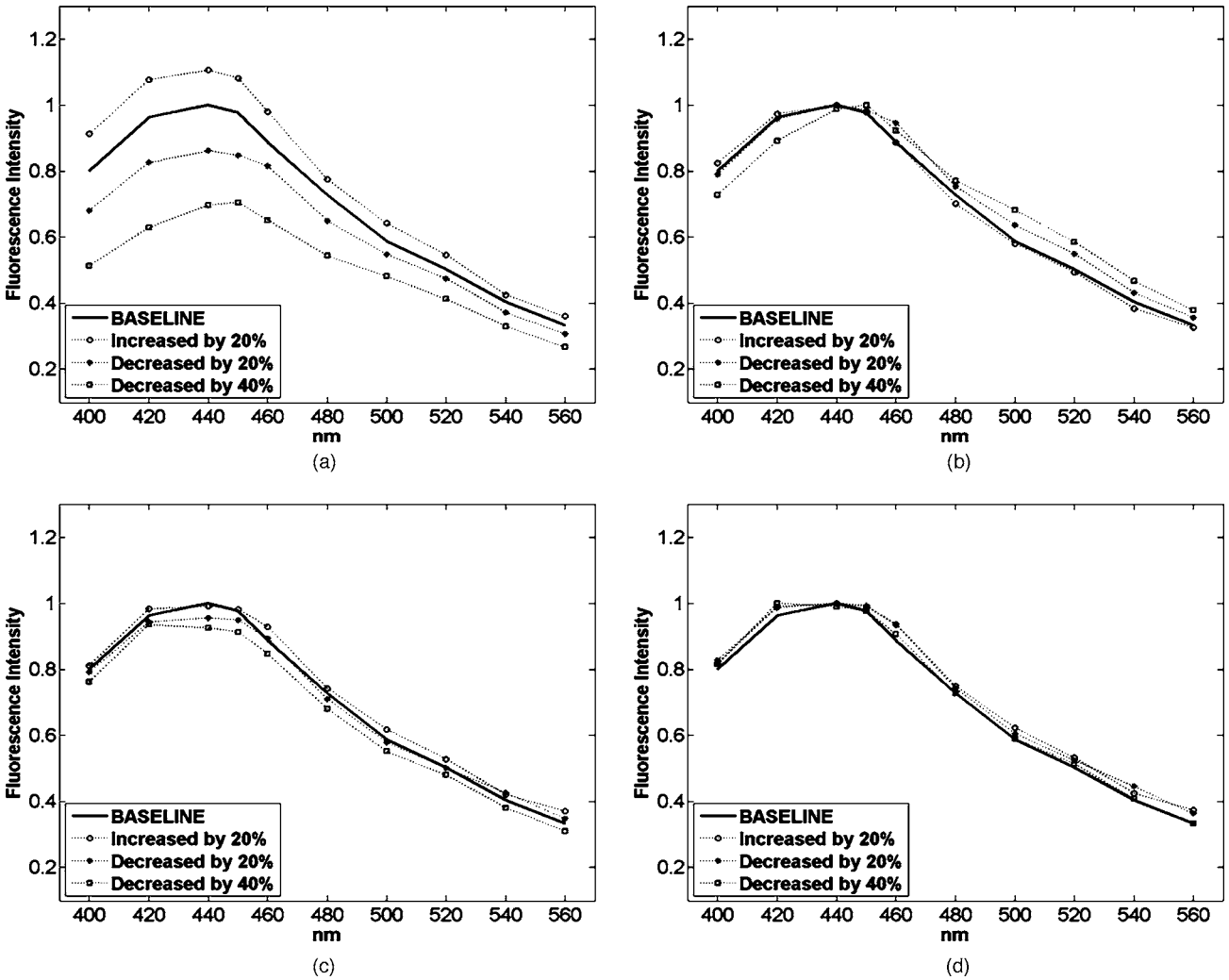


**Fig. 4** Effect of variations in the magnitude of the fluorescence efficiency of the stroma on (a) and (c) the intensity and (b) and (d) spectral shape of the predicted fluorescence spectra: (a) and (b) show changes in superficial stromal layer 1, and (c) and (d) in deeper stromal layer 2.

2. Results indicate that variations in the scattering coefficient in stromal layers 1 and 2 do not change the spectral intensity, shape, or epithelial photons fraction by more then 10%. It should be noted that varying both stromal scattering and hemoglobin absorption had a less pronounced effect on predictions compared to changes associated with variations in the stromal fluorescence and epithelial optical parameters.

### 3.4 *Depth Sensitivity Analysis for Fluorescence Light*

Results in Figs. 4–6 indicate that the fluorescence output is most affected by variations in input parameters from stromal layer 1. This suggests that the modeled probe geometry limits the penetration of excitation light to the superficial layers of the oral mucosa and detects fluorescence that originates mostly from the epithelium and superficial stromal areas. The fraction of superficial fluorescence photons (the number of fluorescence photons originating from the epithelial and superficial stromal layers divided by the total fluorescence photons) was calculated for the baseline case and for simulations with varied epithelial and stromal fluorescence parameters. As shown in Table 1, in the baseline case, 90% of detected fluorescence photons originate from the epithelium and superficial stromal layer 1. While variations in the input parameters influence the value of the superficial photon fraction, results consistently indicate that most (86 to 93%) of the detected fluorescence originates from the epithelium and superficial stroma of the oral mucosa for all sets of simulations.

### 3.5 *Comparison of Average Clinical Fluorescence Spectra from Normal Oral Mucosa and Oral Lesions with Moderate to Severe Dysplasia to Monte Carlo Predictions*

The performance of the Monte Carlo code in predicting normal and abnormal fluorescence spectra was validated by comparing simulation results to average spectra from normal and dysplastic sites measured from the buccal mucosa, the tongue, the lip, and the floor of the mouth at 350-nm excitation. Depth-resolved fluorescence spectra from 281 normal oral sites and 27 oral sites diagnosed with moderate to severe dysplasia were used to calculate the average normal and dysplastic spectra.

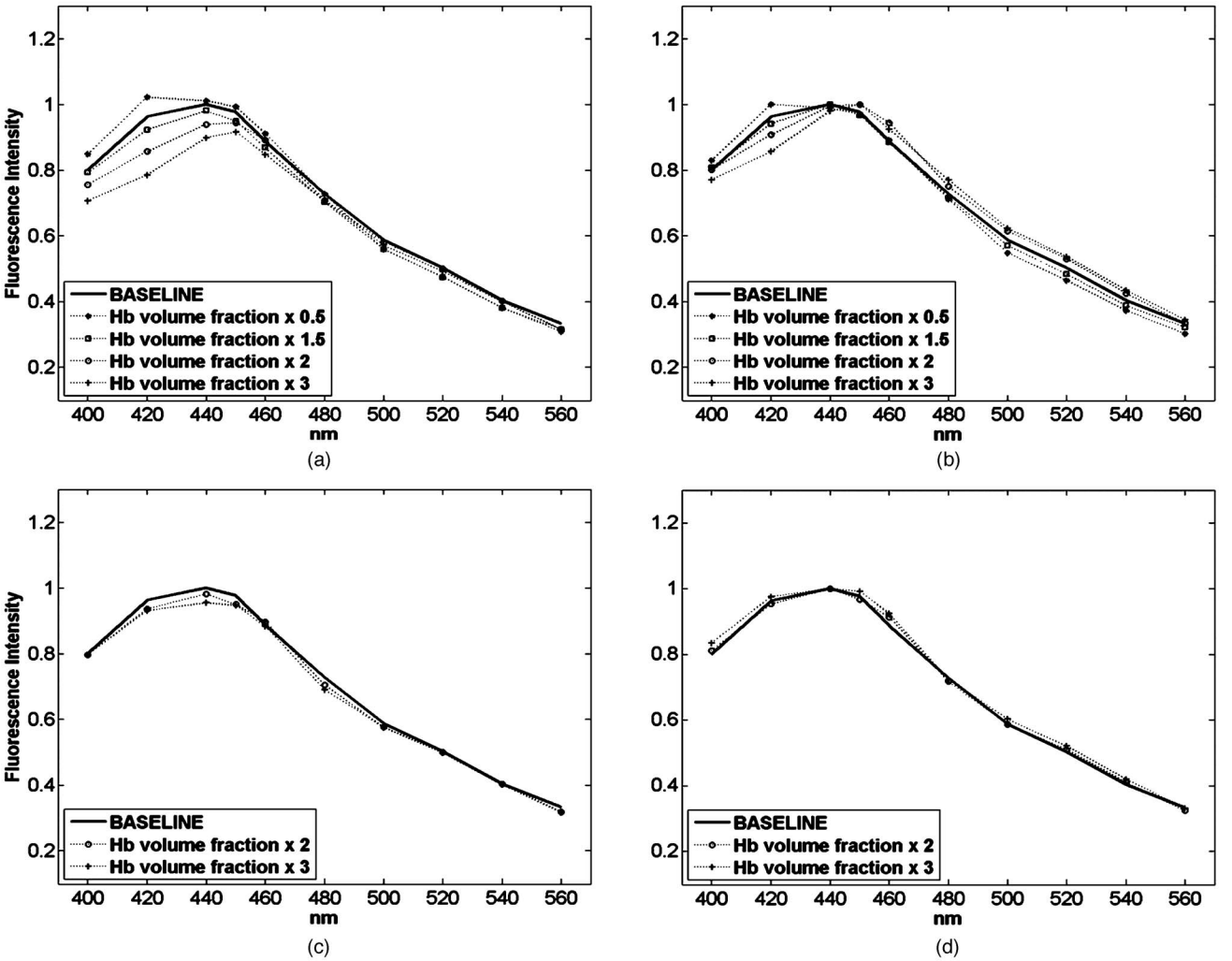


**Fig. 5** Effect of variations in the volume fraction of hemoglobin on (a) and (c) the intensity and (b) and (d) spectral shape of the predicted fluorescence spectra: (a) and (b) show changes in superficial stromal layer 1 and (c) and (d) in deeper stromal layer 2.

Normal oral tissue was simulated with the input parameters and tissue geometry used in the baseline predictions. Dysplasia is characterized by a series of physiological changes, including an increase in the total epithelial thickness (hyperplasia), thickening of the keratinized superficial epithelium, and spreading of abnormal cells with increased scattering and metabolic activity throughout the epithelium. In addition, the fluorescence intensity of superficial stroma was found to decrease in oral lesions diagnosed with dysplasia. Other stromal changes, such as increased Hb absorption and decreased stromal scattering, were not considered because the model sensitivity analysis shows that these parameters have only a small effect on the intensity and shape of predictions. To model dysplastic tissue, the combined effect of changes in the thickness of epithelial sublayers and the fluorescence intensity of subepithelial stoma were considered. Several simulations were performed by varying the thickness of individual epithelial sublayers (data not shown). We find that the set of changes that most closely matches the measured dysplastic fluorescence spectrum is a combination of hyperkeratosis, an increase in the thickness of the basal epithelium to simulate the spreading of metabolically active and highly scattering cells, and a drop of fluorescence intensity of the superficial stroma. In particular, hyperkeratosis was modeled by a small increase in the superficial thickness (70 $\mu$m), a small increase in the thickness of the nonkeratinized epithelium (50 $\mu$m), and an increased fraction of the epithelium occupied by the basal sublayer. The fluorescence intensity of the superficial stromal layer 1 was reduced by a factor of 1.6.

Figure 7 compares the average clinical spectra at 350-nm excitation to simulated spectra from normal and dysplastic sites. The error bars in the figure represent the standard deviation of the clinical average spectra at 420 nm and indicate the degree of variability in the datasets. Results show that the Monte Carlo model is able to predict the drop in intensity and the shift of spectral shape to longer emission wavelengths that accompany dysplastic progression in the clinically measured data. However, it should be mentioned that both the normal and dysplastic simulations are slightly shifted to the red emission region compared to clinical data, suggesting the need for a more precise estimation of the input fluorescence properties

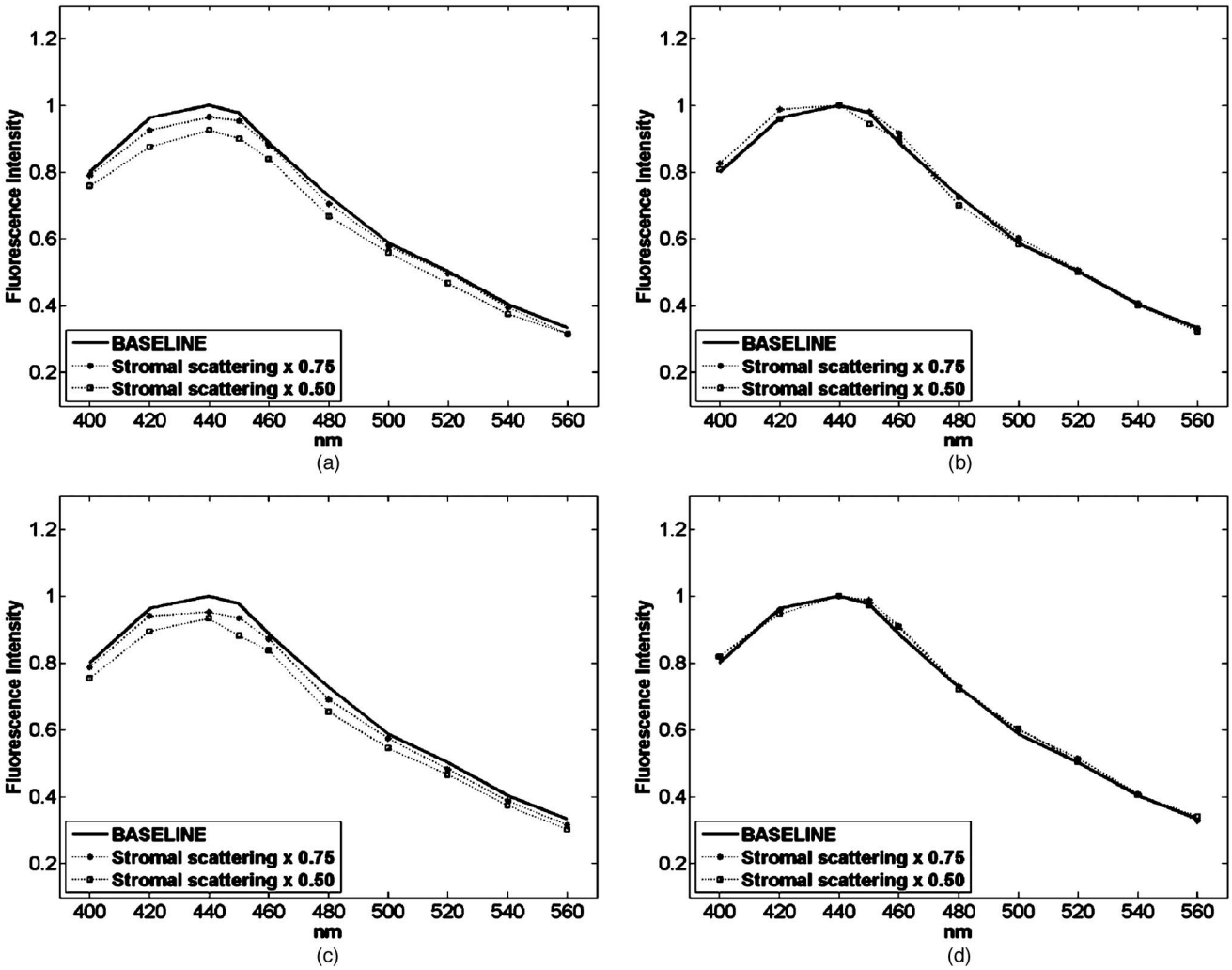


**Fig. 6** Effect of variations in the stromal scattering on (a) and (c) the intensity and (b) and (d) spectral shape of the predicted fluorescence spectra: (a) and (b) show changes in superficial stromal layer 1 and (c) and (d) in deeper stromal layer 2.

for each epithelial sublayer. Bar graphs representing the total number of detected photons from the epithelium and stroma are displayed in Figs. 7(b) and 7(c). The drop in fluorescence intensity can be attributed to a decrease in the total number of photons originating from the stroma, whereas the shift of the emission peak is due to the increased fraction of epithelial photons of the total detected signal.

## 4 Discussion

We present a Monte Carlo forward model to describe the sensitivity of oral tissue spectroscopy data collected with a depth selective fiber optic probe to changes in the optical properties of the epithelium and stroma that accompany the development of dysplasia. Simulation results show that the depth selective probe offers enhanced detection of fluorescence from the superficial layers of the oral mucosa. Spectra from normal and dysplastic oral tissue were simulated using biologically realistic input parameters for tissue geometry and fluorescence intensities for each tissue sublayer. Comparison of simulated spectra to clinical data shows that the model is able to predict the characteristic drop in fluorescence intensity and the shift of spectral shape to longer emission wavelengths that accompanies neoplastic progression in the oral mucosa. Moreover, analysis of the depth of origin of the simulated fluorescence collected with the depth selective probe indicates that the reduced fluorescence intensity associated with dysplasia is due to a decreased number of photons originating from the stroma, whereas the spectral red shift can be attributed to an increase in the fraction of epithelial photons in the total detected signal.

Similar trends in clinical data have been previously reported by other studies on oral cancer detection. For example, previously De Veld et al. found that dysplastic and tumor sites are accompanied by a progressive drop in fluorescence intensity,[7] whereas Lane et al. reported a loss of autofluorescence signal in images of oral precancerous and cancerous lesions compared to the surrounding normal mucosa.[4] Mathematical models for extracting the intrinsic fluorescence spectra from *in-vivo* fluorescence spectra in the cervix[11] and the oral cavity[6] have been previously described. Results from these studies indicate that intrinsic fluorescence spectra can be composed of two spectral components, epithelial (NADH)

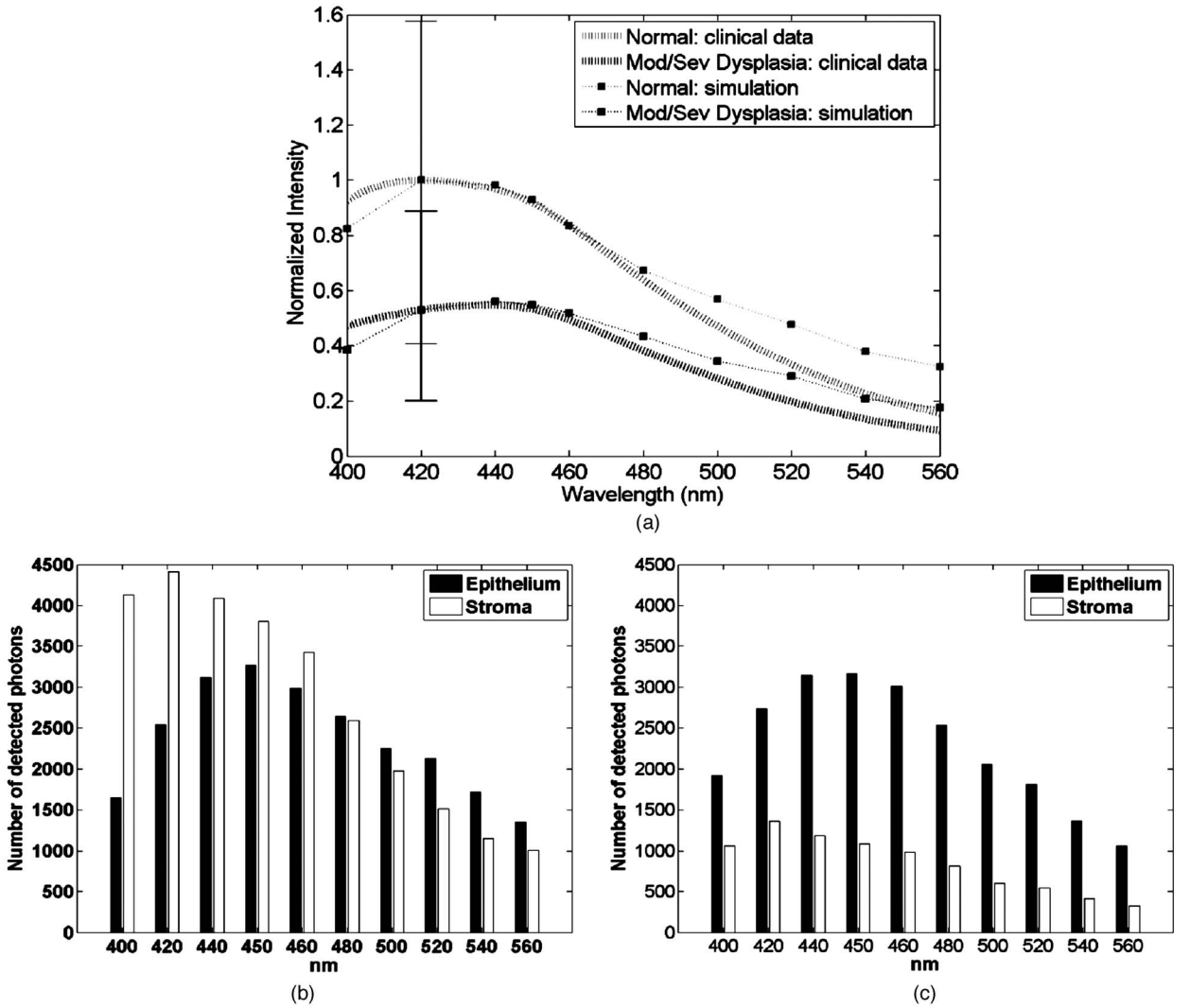


**Fig. 7** Comparison of average clinical fluorescence spectra from normal oral mucosa and lesions diagnosed with moderate to severe dysplasia to Monte Carlo predictions. (a) Average clinical spectra and predictions. Error bars represent the standard deviation in the clinical data for each diagnostic category. Number of detected photons from the epithelium and stroma in (b) normal and (c) dysplastic predictions.

and stromal (collagen), and that the epithelial contribution increases, whereas the stromal contribution decreases with malignant transformation. This is in agreement with current results from the depth analysis of simulated average fluorescence spectra of normal and dysplastic oral tissue.

The model sensitivity analysis described here elucidates the relationship between changes in tissue optical properties commonly associated with neoplastic development, and the spectral characteristics of the depth-resolved fluorescence spectra. It was found that spectra are sensitive to changes in the epithelial properties commonly associated with dysplastic progression in oral tissue. For example, thickening of the epithelial layer, thickening of the keratinized superficial epithelium, and increasing the fraction of the epithelium occupied by more metabolically active and scattering cells all lead to significant changes in the shape and intensity of predicted spectra. As the epithelium becomes thicker and contains more metabolically active cells, the spectral intensity drops and the spectral shape shifts to longer emission wavelengths. These changes are accompanied by an increase in the fraction of epithelial photons in the total detected fluorescence. A major epithelial fluorophore is mitochondrial NADH. In this study, the fluorescence properties of mitochondrial NADH were approximated by emission spectra from SiHa cells in suspension, which have an emission peak at 440 nm. In contrast, collagen cross-links, which are the dominant fluorophores in the stroma, have an emission peak that is more shifted to the blue region (405 nm). Thus, the spectral shift in simulated spectra that is linked to neoplastic changes in oral mucosa suggests that the total detected signal is dominated by NADH-based fluorescence instead of stromal fluorescence.

Previous Monte-Carlo-based model sensitivity analysis of cervical reflectance and fluorescence spectra indicate that changes in epithelial parameters such as epithelial scattering and thickness have only a minimal effect on predictions.[17,18] It should be noted that these studies modeled fluorescence or reflectance detected with optical probes that do not offer en-

hanced detection of epithelial signals. A recent investigation of the autofluorescence properties of viable oral tissue indicates that benign and premalignant lesions have similar stromal but different epithelial fluorescence properties.[21] Thus, depth selective probes, which enhance the sensitivity to epithelial changes, may aid in accurate discrimination of spectra from benign and premalignant lesions.

In particular, results from the penetration depth analysis presented here show that 43 to 66% of total detected light with the depth selective probe originates from the epithelium as the thickness of the nonkeratinized epithelium was varied from 280 to 420 $\mu$m. Previously, a Monte Carlo model without enhanced detection of epithelial signal was employed to simulate fluorescence spectra of cervical tissue and to calculate the fraction of epithelial photons in the total detected fluorescence.[37] Results from this study indicate that more than 80% of the fluorescence originates from the stroma when considering an epithelial thickness of 300 $\mu$m and optical properties similar to those used for the baseline case of normal oral mucosa. In comparison, the Monte Carlo model presented in the current study illustrates that the depth selective probe offers a significant improvement in detecting light from the epithelial layer.

However, results from the depth sensitivity analysis also indicate that the modeled probe does not offer complete rejection of stromal fluorescence. This is in agreement with experimental measurements of the depth sensitive collection efficiency of the clinical probe, which indicate that even though the probe's response is weighted toward the epithelium, it cannot completely exclude stromal signals.[16] Moreover, the simulations presented here indicate that most of the stromal fluorescence originates from the superficial stromal region and not from deeper stroma. For example, the fraction of photons originating from the epithelium and superficial stromal regions varies from 88 to 93%, depending on the epithelial thickness. Changes in the optical properties of deeper stroma, such as increased hemoglobin concentration and decreased stromal scattering and fluorescence intensity, have minimal effect on predicted fluorescence spectra.

The relevance of Monte Carlo models in predicting and analyzing clinical data depends significantly on the chosen input parameters. We have shown that predictions with the depth sensitive Monte Carlo model are influenced by the tissue geometry and fluorescence properties of the superficial oral mucosa (the epithelial layer and the superficial stromal region). Therefore, valid predictions of depth-enhanced spectra from the oral cavity depend on the use of input parameters that accurately represent the tissue geometry and the fluorescence properties of the interrogated tissue. A major advantage of the Monte Carlo model described in this work is the use of realistic tissue geometries derived from confocal images of viable oral tissue. However, it should be noted that the tissue geometry used to simulate the average dysplastic spectrum was not intended to represent a specific oral lesion site. For example, some oral lesions are expected to have keratin layers that are thicker than the values used here, which, as suggested by the model sensitivity analysis, may significantly reduce the predicted spectral intensity. Thus, accurate application of the depth sensitive Monte Carlo model in predicting site-specific spectra would depend on prior knowledge of the tissue geometry for the particular lesion of interest. In addition, some of the assumptions made in this model, about the major fluorophores and spectral characteristics of each sublayer, may affect the accuracy of predictions. We speculate that the difference in predicted and clinically measured spectra in the 500- to 560-nm region is caused by overestimating the contribution of FAD (the assumed fluorophore in the intermediate epithelium) to the total detected fluorescence. The fluorescence patterns of the intermediate epithelium, observed in confocal images of oral tissue (weak cytoplasmic fluorescence at UV excitation but an increased cytoplasmic fluorescence at 488 nm compared to basal epithelium), suggested that the major fluorophore in this layer is FAD. However, it is also possible that this layer has contributions of both FAD and NADH, which would improve agreement between predicted and measured average spectra. Thus, a more direct technique for estimating the spectral characteristics of the epithelial sublayers, such as measuring fluorescence spectra directly from the confocal images of tissue slices by means of spectral imaging, could significantly improve the accuracy of the predictions. It should also be mentioned that the input for the volume fraction of stromal hemoglobin was estimated from previous studies on cervical and colon tissue. A more accurate estimation of the volume fraction of hemoglobin in the subepithelial stroma of oral tissue can also lead to improved predictions of depth-resolved fluorescence spectra.

## Acknowledgment

This work was supported by NIH grant R01 CA095604.

## References

1. C. S. Betz, M. Mehlmann, K. Rick, H. Stepp, G. Grevers, R. Baumgartner, and A. Leunig, "Autofluorescence imaging and spectroscopy of normal and malignant mucosa in patients with head and neck cancer," *Lasers Surg. Med.* **25**, 323–334 (1999).
2. R. Paczona, S. Temam, F. Janot, P. Marandas, and B. Luboinski, "Autofluorescence videoendoscopy for photodiagnosis of head and neck squamous cell carcinoma," *Eur. Arch. Otorhinolaryngol.* **260**, 544–548 (2003).
3. B. Kulapaditharom and V. Boonkitticharoen, "Performance characteristics of fluorescence endoscope in detection of head and neck cancers," *Ann. Otol. Rhinol. Laryngol.* **110**, 45–52 (2001).
4. P. M. Lane, T. Gilhuly, P. Whitehead, H. Zeng, C. F. Poh, S. Ng, P. M. Williams, L. Zhang, M. P. Rosin, and C. E. MacAulay, "Simple device for the direct visualization of oral-cavity tissue fluorescence," *J. Biomed. Opt.* **11**, 024006 (2006).
5. D. L. Heintzelman, U. Utzinger, H. Fuchs, A. Zuluaga, K. Gossage, A. M. Gillenwater, R. Jacob, B. Kemp, and R. R. Richards-Kortum, "Optimal excitation wavelengths for *in vivo* detection of oral neoplasia using fluorescence spectroscopy," *Photochem. Photobiol.* **72**, 103–113 (2000).
6. M. G. Muller, T. A. Valdez, I. Georgakoudi, V. Backman, C. Fuentes, S. Kabani, N. Laver, Z. Wang, C. W. Boone, R. R. Dasari, S. M. Shapshay, and M. S. Feld, "Spectroscopic detection and evaluation of morphologic and biochemical changes in early human oral carcinoma," *Cancer* **97**, 1681–1692 (2003).
7. D. C. G. de Veld, M. Skurichina, M. J. H. Witjes, R. P. W. Duin, H. J. C. M. Sterenborg, and J. L. N. Roodenburg, "Autofluorescence and diffuse reflectance spectroscopy for oral oncology," *Lasers Surg. Med.* **36**, 356–354 (2005).
8. D. C. G. de Veld, M. Skurichina, M. J. H. Witjes, R. P. W. Duin, H. J. C. M. Sterenborg, and J. L. N. Roodenburg, "Clinical study for classification of benign, dysplastic and malignant oral lesions using autofluorescence spectroscopy," *J. Biomed. Opt.* **9**(5), 940–950 (2004).
9. Q. Liu and N. Ramanujam, "Sequential estimation of optical properties of a two-layered epithelial tissue model from depth-resolved ultraviolet-visible diffuse reflectance spectra," *Appl. Opt.* **45**, 4776–4790 (2006).

10. J. C. Finlay and T. H. Foster, "Recovery of hemoglobin oxygen saturation and intrinsic fluorescence with a forward-adjoint model," *Appl. Opt.* **44**, 1917–1933 (2005).
11. I. Georgakoudi, B. C. Jacobson, M. G. Muller, E. E. Sheets, K. Badizadegan, D. L. Carr-Locke, C. P. Crum, C. W. Boone, R. R. Dasari, J. Van Dam, and M. S. Feld, "NAD(P)H and collagen as *in vivo* quantitative fluorescent biomarkers of epithelial precancerous changes," *Cancer Res.* **62**, 682–687 (2002).
12. S. K. Chang, N. Marin, M. Follen, and R. Richards-Kortum, "Model-based analysis of clinical fluorescence spectroscopy for in-vivo detection of cervical intraepithelial dysplasia," *J. Biomed. Opt.* **11**, 024008 (2006).
13. L. Nieman, A. Myakov, J. Aaron, and K. Sokolov, "Optical sectioning using a fiber probe with an angled illumination-collection geometry: evaluation in engineered tissue phantoms," *Appl. Opt.* **43**, 1308–1319 (2004).
14. C. Zhu, Q. Liu, and N. Ramanujam, "Effect of fiber optic probe geometry on depth-resolved fluorescence measurments from epithelial tissues: a Monte Carlo simulation," *J. Biomed. Opt.* **8**(2), 237–247 (2003).
15. D. Arifler, R. A. Schwarz, S. K. Chang, and R. Richards-Kortum, "Reflectance spectroscopy for diagnosis of epithelial precancer: model-based analysis of fiber-optic probe designs to resolve spectral information from epithelium and stroma," *Appl. Opt.* **44**, 4291–4305 (2005).
16. R. A. Schwarz, W. Gao, D. Daye, M. D. Williams, R. Richards-Kortum, and A. Gillenwater, "Autofluorescence and diffuse reflectance spectroscopy of oral epithelial tissue using a depth-sensitive fiber-optic probe," *Appl. Opt.* **47**, 825–834 (2008).
17. S. K. Chang, D. Aflifer, R. Drezek, M. Follen, and R. Richards-Kortum, "Analytical model to describe fluorescence spectra of normal and preneoplastic epithelial tissue: comparison with Monte Carlo simulations and clinical measurements," *J. Biomed. Opt.* **9**(3), 511–522 (2004).
18. D. Arifler, C. MacAulay, M. Follen, and R. Richards-Kortum, "Spatially resolved reflectance spectroscopy for diagnosis of cervical precancer: Monte Carlo modeling and comparison to clinical measurements," *J. Biomed. Opt.* **11**, 064027 (2006).
19. D. Hidovic-Rowe and E. Claridge, "Modeling and validation of spectral reflectance for the colon," *Phys. Med. Biol.* **50**, 1071–93 (2005).
20. J. Y. Qu, C. E. MacAulay, S. Lam, and B. Palcic, "Laser-induced fluorescence spectroscopy at endoscopy: tissue optics, Monte Carlo modeling, and *in vivo* measurements," *Opt. Eng.* **34**(11), 3334–3343 (1995).
21. I. Pavlova, M. Williams, A. El-Naggar, R. Richards-Kortum, and A. Gillenwater, "Understanding the biological basis of autofluorescence imaging for oral cancer detection: High resolution fluorescence microscopy in viable tissue," *Clin. Cancer Res.* **14**, 2396–2404 (2008).
22. T. Collier, M. Follen, A. Malpica, and R. Richards-Kortum, "Sources of scattering in cervical tissue: determination of the scattering coefficient by confocal microscopy," *Appl. Opt.* **44**, 2072–81 (2005).
23. A. L. Clark, A. Gillenwater, R. Alizadeh-Naderi, A. K. El-Naggar, and R. Richards-Kortum, "Detection and diagnosis of oral neoplasia with an optical coherence microscope," *J. Biomed. Opt.* **9**(6), 1271–80 (2004).
24. M. C. Skala, J. M. Squirrell, K. M. Vrotsos, J. C. Eickhoff, A. Gendron-Fitzpatrick, K. W. Eliceiri, and N. Ramanujam, "Multiphoton microscopy of endogenous fluorescence differentiates normal, precancerous, and cancerous squamous epithelial tissues," *Clin. Cancer Res.* **65**, 1180–1186 (2005).
25. D. E. Ingber, "Cancer as a disease of epithelial-mesenchymal interactions and extracellular matrix regulation," *Differentiation* **70**, 547–560 (2002).
26. D. Arifler, I. Pavlova, A. Gillenwater, and R. Richards-Kortum, "Light scattering from collagen fiber networks: micro-optical properties of normal and neoplastic stroma," *Biophys. J.* **92**, 3260–3274 (2007).
27. S. Pazouki, D. M. Chisholm, M. M. Adi, G. Carmichael, M. Farquharson, G. R. Ogden, S. L. Schor, and A. M. Schor, "The association between tumour progression and vascularity in the oral mucosa," *J. Pathol.* **183**, 39–43 (1999).
28. K. Sokolov, J. Galvan, A. Myakov, A. Lacy, R. Lotan, and R. Richards-Kortum, "Realistic three-dimensional epithelial tissue phantoms for biomedical optics," *J. Biomed. Opt.* **7**(1), 148–156 (2002).
29. J. Qu, C. MacAulay, S. Lam, and B. Palcic, "Optical properties of normal and carcinomatous bronchial tissue," *Appl. Opt.* **33**, 7397–7405 (1994).
30. J. R. Mourant, J. P. Freyer, A. H. Hielscher, A. A. Eick, D. Shen, and T. M. Johnson, "Mechanisms of light scattering from biological cells relevant to noninvasive optical-tissue diagnostics," *Appl. Opt.* **37**, 3586–3593 (1998).
31. S. L. Jacques, *Skin Optics*, Oregon Medical Laser Centre, Portland, OR (1998), see http://omlc.ogi.edu/news/jan98/skinoptics.html.
32. G. Zonios, L. T. Perelman, V. Backman, R. Manoharan, M. Fitzmaurice, J. Van Dam, and M. S. Feld, "Diffuse reflectance spectroscopy of human adenomatous colon polyps *in vivo*," *Appl. Opt.* **38**, 6628–6637 (1999).
33. I. S. Saidi, "Transcutaneous optical measurement of hyperbilirubinemia in neonates," PhD Dissertation, Rice University, Houston, TX (1992).
34. S. L. Jacques and L. Wang, "Monte Carlo modeling of light transport in tissues," in *Optical-Thermal Response of Laser-Irradiated Tissue*, A. J. Welch and M. J. C. van Gemert, Eds., pp. 78–79, Plenum, New York (1995).
35. A. J. Welch, C. Gardner, R. Richards-Kortum, E. Chan, G. Criswell, J. Pfefer, and S. Warren, "Propagation of fluorescent light," *Lasers Surg. Med.* **21**, 166–178 (1997).
36. M. Macluskey, L. M. Chandrachud, S. Pazouki, M. Green, D. M. Chisholm, G. R. Ogden, S. L. Schor, and A. M. Schor, "Apoptosis, proliferation, and angiogenesis in oral tissue. Possible relevance to tumor progression," *J. Pathol.* **191**, 368–375 (2000).
37. R. Drezek, K. Sokolov, U. Utzinger, I. Bioko, A. Malpica, M. Follen, and R. Richards-Kortum, "Understanding the contributions of NADH and collagen to cervical tissue fluorescence spectra: Modeling, measurements, and implications," *J. Biomed. Opt.* **6**(4), 385–396 (2001).